



Trapping of Suspended Sediment by Submerged Aquatic Vegetation in a Tidal Freshwater Region: Field Observations and Long-Term Trends

Paul A. Work¹ · Maureen Downing-Kunz¹ · Judith Z. Drexler¹

Received: 31 January 2020 / Revised: 24 June 2020 / Accepted: 3 July 2020

© This is a U.S. government work and not under copyright protection in the U.S.; foreign copyright protection may apply 2020

Abstract

Widespread invasion by non-native, submerged aquatic vegetation (SAV) may modify the sediment budget of an estuary, reducing the availability of inorganic sediment required by marshes to maintain their position in the tidal frame. The instantaneous trapping rate of suspended sediment in SAV patches in an estuary has not previously been quantified via field observations. In this study, flows of water and suspended sediment through patches of invasive SAV were measured at three tidally forced, freshwater sites, all located within the Sacramento-San Joaquin Delta in California. An acoustic Doppler current profiler deployed from a roving vessel provided velocity and backscatter data used to quantify fluxes of both water and suspended sediment. Sediment trapping efficiency, defined as instantaneous net trapped flux divided by incident flux, was positive in 24 of 29 cases, averaging +5%. Coupled with 3 years of measured sediment flux data at one site, this suggests that trapping averages $3.7 \text{ kg m}^{-2} \text{ year}^{-1}$. This estimate compares favorably with the mean mass accumulation rate of $3.8 \text{ kg m}^{-2} \text{ year}^{-1}$ estimated from dated sediment cores collected at the study sites. Long-term measurements made upstream reveal a strong negative trend ($-1.8\% \text{ year}^{-1}$) in suspended sediment concentration, and intra-annual changes in both suspended sediment concentration and percent fines. The large footprint and high spatial density of invasive SAV coupled with declining sediment supply are diminishing downstream suspended sediment concentrations, potentially reducing the resiliency of marshes in the Delta and lower estuary to future sea-level rise.

Keywords Invasive aquatic vegetation · Hydrodynamics · Suspended sediment · Tidal velocity · Tidal marsh · *Egeria densa*

Introduction

Sediment budgets are often quantified to reveal whether river reaches, estuaries, or coastal regions are gaining or losing sediment (e.g., Ganju et al. 2013). Tidal marshes typically require an influx of inorganic sediment to maintain their position in the tidal frame (Vogel et al. 1996; Turner et al. 2001; Drexler 2011), and a sediment budget helps assess whether a

planned tidal marsh restoration has a high likelihood for success (Ganju et al. 2019). Changes in land and water management activities can alter the supply and pathways of sediment traveling downstream. An increase in abundance of invasive submerged aquatic vegetation (SAV) in a waterway can likewise modify how water and sediment move through an aquatic environment (Champion and Tanner 2000) and may affect the overall availability of suspended sediment in an estuary (Hestir et al. 2016).

The magnitude of sediment trapping by aquatic macrophytes including SAV depends on many variables including incident flow conditions, incident sediment flux, and characteristics of the bed and vegetation. For SAV, most studies have focused on how seagrasses and a few freshwater SAV species obstruct flow or alter the process of sediment deposition on a channel bed (Getsinger and Dillon 1984; Lacy and Wyllie-Echeverria 2011; Jones et al. 2012; Nepf 2012; Sand-Jensen 1998). Little if any attention has been devoted to the actual trapping efficiency of the vegetation itself.

Communicated by Mead Allison

Electronic supplementary material The online version of this article (<https://doi.org/10.1007/s12237-020-00799-w>) contains supplementary material, which is available to authorized users.

✉ Paul A. Work
pwork@usgs.gov

¹ U.S. Geological Survey, California Water Science Center, Sacramento, CA, USA

Many studies related to marsh restoration and sea-level rise in both salt and freshwater marshes provide relevant findings, although results are often expressed as sediment erosion or deposition rates that do not reveal trapping efficiency and often do not include detailed measurements of flow or suspended sediment characteristics. Sheehan and Ellison (2015) studied marsh sites subsequent to removal of the macrophyte *Spartina anglica* and found a sixfold increase in erosion rate. Darke and Megonigal (2003) concluded that freshwater marsh vegetation was an important factor in controlling sediment deposition when sediment deposition was not limited by incident supply.

Van der Deijl et al. (2017) considered sediment trapping within two polders over separate 9–10-month periods and found a decrease in sediment trapping efficiency as winds and flow rates increased, in turn increasing bed shear stresses. Flow inlets and outlets were monitored with fixed turbidity sensors and flowmeters to quantify sediment fluxes at 10-min intervals. A wide range of trapping efficiencies was reported, with time-averaged values for the two sites of +29 and –10%. They used the method of Asselman and Van Wijngaarden (2002) to estimate theoretical maximum trapping efficiencies of 72 and 80% for the two sites. These theoretical upper bounds were based on a very simple one-dimensional settling basin analogy, considering only sediment settling velocity, basin area, and inflow rate.

Dense patches of SAV in channel environments will modify planform flow patterns, velocity profiles, and turbulent intensities of the flow. Nepf (2012) notes that within dense canopies, the flow can be considered two regions, with the lower region experiencing reduced transport and turbulence with a length scale dictated by the stem size and relative spacing of the vegetation. The relative thicknesses of the flow layers are controlled by the drag of the canopy on the flow.

Sediment suspended in the water column is pulled downward by gravity but elevated periodically by turbulent excursions that scale with the flow speed (e.g., Rouse 1937). If SAV slows the flow sufficiently, and turbulence is reduced, gravity dominates, and the sediment will settle to the bed (Getsinger and Dillon 1984; Petticrew and Kalff 1992; Wilcock et al. 1999; Hestir et al. 2013; Hestir et al. 2016). The sediment may also be intercepted by the SAV itself.

Other factors that affect sediment trapping include characteristics of the SAV and sediment itself. The type, distribution, and horizontal leaf area index of the SAV will influence how much of the flow passes through the vegetated region (Nepf 2012, Kim et al. 2018). Thick vegetation will reduce sediment flux into a canopy but make it more effective at trapping the sediment that does enter, since reduced turbulence will favor sediment settling.

Characteristics of the suspended sediment, including density, composition, and grain size distribution are often not reported but can affect the sediment concentration profile

and therefore susceptibility to trapping. Time dependence in discharge and water level are also important because of the nonlinear relationship between flow speed and flow-induced shear stresses. Note that throughout this paper, the term “discharge” is used to refer to the complete volumetric flowrate within a channel, whereas the term “water flux” is used to describe flow through a subsection of the channel.

In order to estimate sediment trapping in SAV, it is necessary to first obtain an accurate measurement of suspended sediment transport, which is challenging. Often, optical (Rasmussen et al. 2009) or acoustic (Landers et al. 2016) proxies are used to quantify suspended sediment concentration (SSC) at a point, which is then empirically converted to a cross-sectional average, and multiplied by measured water discharge to arrive at the total, instantaneous sediment flux in a channel. Uncertainty in SSC is typically much higher than uncertainty in water discharge. The optical sensors most often used are very sensitive to biological fouling, leading to gaps in measured time series, but are still in widespread use for real-time observations.

Acoustic techniques have two major advantages over optical approaches for estimating SSC. One is that the former is much less influenced by biological fouling, which is important for long-term measurement campaigns. The other is that acoustic backscatter can be evaluated at different distances from the sound source, allowing estimates of concentration profiles (Vergne et al. 2020). For these reasons, the interest in and application of acoustic sensors for estimation of SSC has increased to a point where a commercial acoustic sensor is now available for this purpose, and sensors are routinely being deployed in both research and operational modes in both marine and fresh water environments (Chanson et al. 2008; Landers et al. 2016; Ozturk 2018; Vergne et al. 2020). Regardless of sensor type, it is important to validate by comparison with estimates derived from water bottle samples.

Computational fluid mechanics tools have been applied to study flow and sediment transport in and near SAV, but it is a challenging fluid-structure interaction scenario represented by flow through a waving SAV canopy and complicated sediment dynamics. Numerical models have been applied to the case of sediment transported into SAV by both flowing water (Kim et al. 2018) and flowing air (Gonzales et al. 2018), but modeling approaches require measurements for both input and validation, and these are not easily obtained, particularly in the field. Many previous investigations of flow through, over or past SAV have neglected movement and time dependence of the SAV geometry, in many cases replacing the SAV with rigid, inorganic models (Gross 1987; Huthoff et al. 2007; Tanino and Nepf 2008; Stoesser et al. 2010; Zong and Nepf 2011; Chang and Constantinescu 2015). Some have employed two-dimensional (Kim et al. 2018) or analytical (Huthoff et al. 2007) solutions to simplify the problem. Some focus on changes in sediment deposition and erosion patterns outside of vegetated areas.

Deposition and erosion processes of fine sediments are typically modeled using separate critical shear stresses for erosion and deposition, and these can be time dependent and are often assumed or measured with low certainty (Walder 2015). A sediment budget approach that identifies inflows and outflows and assumes conservation of mass to quantify trapping removes the need for detailed inspection or simulation of processes taking place within the domain and the resulting cumulative uncertainty.

This paper focuses on three aspects of sediment transport within a freshwater tidal region, as follows: (1) the instantaneous rates at which sediment is trapped by SAV, (2) long-term changes in the supply of sediment reaching the SAV, and (3) the effects of both of these processes on the long-term, large-scale sediment budget for the estuary. Field observations dating back to the 1940s combined with newer assessments of sediment trapping efficiency derived from mobile acoustic sensors form the basis for the conclusions. The main hypothesis of this paper is that instantaneous field observations of sediment trapping can be made and scaled up in space and time to reveal the long-term, large-scale impacts of invasive SAV on sediment transport in an estuary.

Study sites are in the Sacramento-San Joaquin River Delta (Delta) in northern California, which is an intensely studied and heavily modified estuary (Wright and Schoellhamer 2005, Hestir et al. 2013). The region has been heavily impacted by invasive aquatic vegetation, particularly the floating aquatic plant, water hyacinth (*Eichhornia crassipes* Mart.), and the submerged aquatic plant, Brazilian waterweed (*Egeria densa* Planch.) (Durand et al. 2016). Previous research has suggested that invasive SAV is capable of trapping sediment (Hestir et al. 2016); here, we present the first direct, instantaneous measurements of sediment trapping and assess the long-term implications of such changes on the sediment dynamics of the greater estuary.

Methodology

Site Description

The Delta footprint spans 2400 km², most of it currently utilized for agriculture. It receives freshwater inputs from two primary sources, the Sacramento River to the north, and the San Joaquin River to the south, with watershed areas estimated at 60,900 and 35,060 km², respectively (Wright and Schoellhamer 2005). Water exports for municipal, industrial and agricultural use are at times a significant fraction of the freshwater inflow, but the remainder eventually travels through the narrow Carquinez Strait into San Francisco Bay. Most Delta tributaries were dammed in the twentieth century, resulting in reductions in peak flows and augmentation of low summer flows. Salinity is typically in the range 0–15, with strong seasonal variability. The entire region is subject to

semidiurnal tides, with range 0.6–1.8 m (Ingebritsen et al. 2000; Wright and Schoellhamer 2005).

Instantaneous trapping of suspended sediment was measured in three distinctly different channels within the Delta (Fig. 1). The SAV patches considered here are composed primarily of Brazilian waterweed and are found in water with depth less than ~1.2 m at low tide. They are fixed in space and typically span the entire water column at low tide (Durand et al. 2016).

Some of the surveyed patches lie against channel banks; others are detached and appear as vegetated shoals (Fig. 2). Within the study area, invasive SAV patches have grown considerably over the past two decades, and as of 2015 blanketed over 21 km², one third of Delta waterways (Khanna et al. 2019). Many patches are only tens of meters in length, but some completely cover areas that filled with water when levees protecting subsided islands failed. The focus of the field measurement effort was on the smaller patches that experience bidirectional flows driven by astronomical tides and storm runoff events.

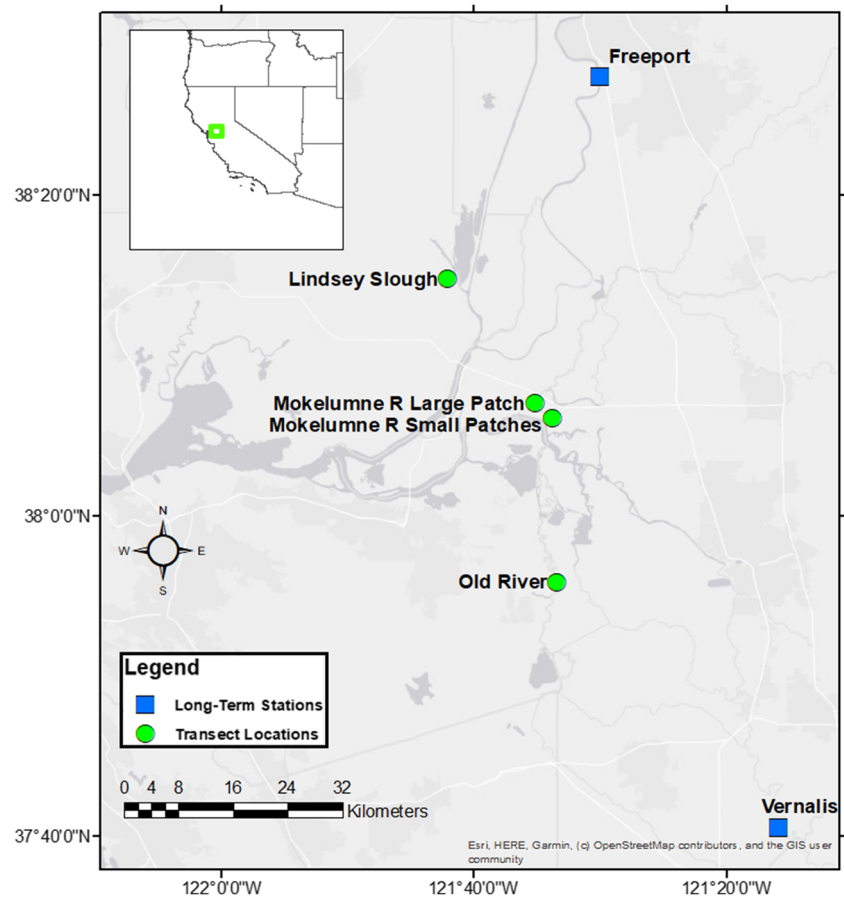
Estimation of Instantaneous Trapping of Suspended Sediment

Data describing fluxes of water and suspended sediment through patches of SAV were collected at three locations in the Delta region (Fig. 1), as follows: (1) Lindsey Slough, a dead-end channel from which agricultural water supply is taken near the upstream end and featuring a very small watershed, (2) Mokelumne River, which has strong net flow in the ebb tidal direction during storm events, and (3) Old River, which has its net flow direction periodically reversed by pumping for California's Central Valley and State Water Projects. All three sites are subject to micro-tidal, semidiurnal tides. Site coordinates and other data can be found in Downing-Kunz et al. (2019).

A patch of SAV, and the shoal upon which it often sits, represents an obstacle to the incident flow. Some flow will be diverted around it, but some will pass through or over the SAV (Nepf 2012). Sediment may be deposited within the SAV, or eroded from within the patch, depending on flow conditions, suspended sediment concentration, vegetation spatial density, geometry, and depositional history at the site. If velocity measurements are made throughout the water column along a closed loop transect, in steady flow, conservation of mass requires that the net flux through the loop be zero, regardless of the transect path followed. This net flux can be written in terms of boat and water velocity vectors \vec{V}_b and \vec{V}_w as:

$$Q = \int_0^T \int_0^d (\vec{V}_w \times \vec{V}_b) \cdot \hat{k} dz dt \quad (1)$$

Fig. 1 Study site locations in the Delta. Pumping stations for the Central Valley and State Water Projects are located just south of the Old River site, to export water south via aqueducts. In the absence of this pumping, net flow is from east to west, toward Suisun Bay at the left, and then into San Francisco Bay



Here, Q is net water flux (volume per unit time) through the non-circular, right cylinder lying between the vessel's closed track along the water surface and the riverbed. The integration spans the time interval T over which the transect data are collected, and the full extent of the water column, which has

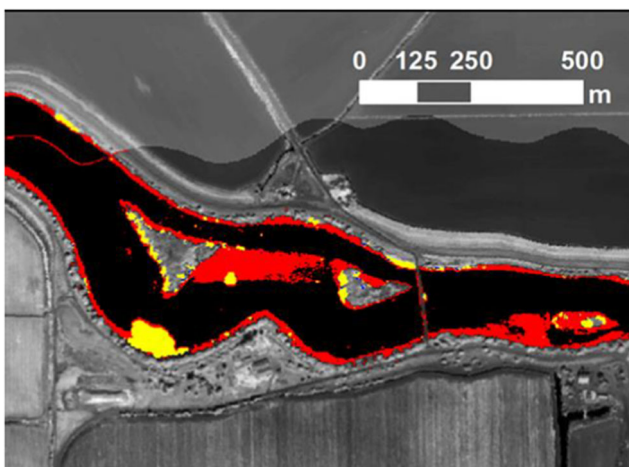


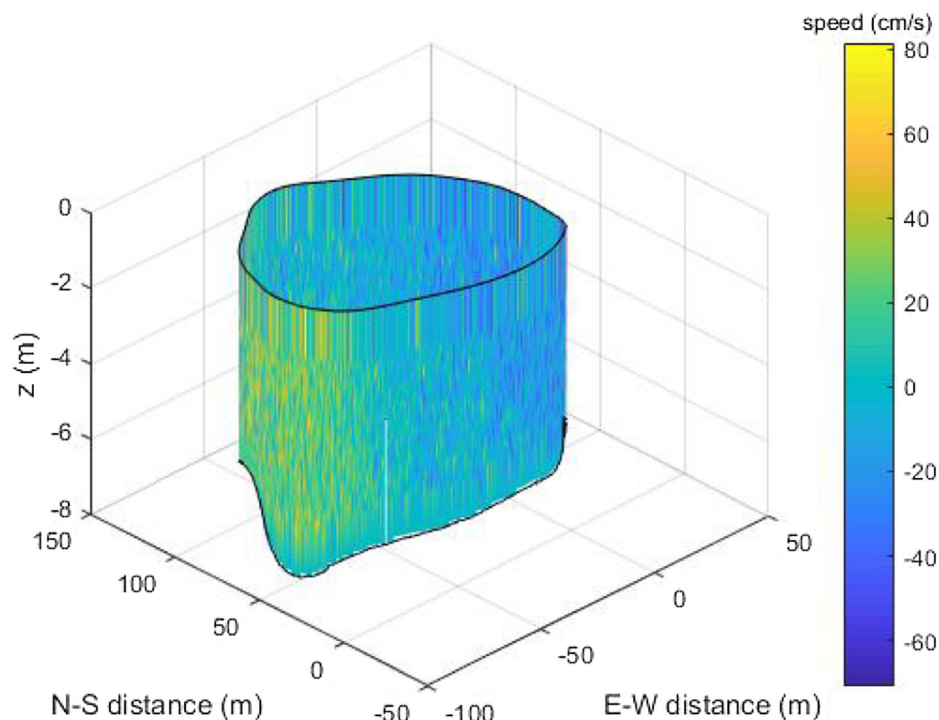
Fig. 2 False color image based on remote sensing showing invasive floating aquatic vegetation (yellow) and SAV (red) at Lindsey Slough in the Sacramento-San Joaquin Delta in California. Gray regions are subaerial; black denotes surface water with no detected vegetation

variable depth d . The unit vector \hat{k} points upward from the water surface (Simpson and Oltmann 1993). This approach can also be used for an arced transect that starts and ends at two points on the same river bank, since the net flow through this track, if steady, must also be zero. Since the surveyed sites are all forced by semi-diurnal tides, measurements were completed within 15 min to avoid severely violating the steady flow assumption.

Acoustic Doppler velocity meters (1200 kHz; RD Instruments Workhorse and River Pro models) were used to obtain both velocity and acoustic backscatter data in the field, typically deployed from a custom inflatable kayak to minimize instrument and vessel draft. The kayak would circumnavigate a patch of SAV, maneuvering to avoid drifting inside the patch, because SAV interferes with the acoustic signal used for measurements and leads to gaps in the data. Figure 3 shows one loop that was measured as a test case.

If the parentheses in Eq. (1) are replaced with absolute value notation, the resulting computed quantity is the gross flux of water beneath the boat. The ratio of the computed net water flux to the gross water flux, ideally zero for a closed loop, was taken as a dimensionless measure of data quality. In this instance this ratio was 1%, with a corresponding mean velocity of less than 2 mm s^{-1} , well below the instrument

Fig. 3 Top, 3D visualization of flow measured along closed-loop transect in open water, Lindsey Slough, California, 11 January 2017, 13:08 PST, flood tide. Vertical datum is at water surface and horizontal datum (0.,0) at transect starting point. This figure shows only the component of velocity normal to the surface of the cylinder defined by the boat track. Velocities have been extrapolated up and down outside of the measured zone to span the entire water column. Bottom, planform view of same track, with velocity vectors averaged over the vertical within the measurement zone shown. Only every tenth measured vector is shown



manufacturer’s rated uncertainty of $3 \text{ mm s}^{-1} + 0.3\%$ of velocity relative to the instrument head. Bottom tracking and the instrument’s electromagnetic compass were used to define required positioning and heading information.

For a given flow speed, a longer or deeper transect will result in a larger computed gross flux, which will tend to reduce the ratio of net to gross flux, if errors are Gaussian. Transect area ranged from 650 to 8600 m^2 , but there was no correlation between the net to gross flux ratio and transect area ($R^2 = 0.003$, $n = 35$, $p = 2.8\text{e-}08$).

Results where net water flux divided by gross flux exceeded 15% were excluded from consideration. The

resulting dataset featured 29 observations, with the mean and median values of the water flux ratio 7% and 6% , respectively. The net flux of water was treated as measurement error and distributed in equal parts to the inflow and outflow portions of the transect to force the net water flux to zero:

$$Q_w^+ = Q_{w_{\text{raw}}}^+ - \frac{\Delta Q_w}{2} \tag{2}$$

$$Q_w^- = Q_{w_{\text{raw}}}^- - \frac{\Delta Q_w}{2} \tag{3}$$

where ΔQ_w is the error in the computed net water flux, Q_w^+ is the water flux in, and Q_w^- the water flux out of the control

volume. Flux into the surveyed loop is defined as positive. The subscript raw denotes a computed quantity prior to the application of any corrections.

The acoustic backscatter signal, recorded simultaneously with the velocity data, and featuring identical resolution, was used to compute sediment concentration along the looped transects. It was assumed that there is a unique, site-specific relation between acoustic backscatter and SSC (Landers et al. 2016). A P61 point-integrating sampler (Edwards and Glysson 1999, Federal Interagency Sedimentation Project 2015) was deployed at two sites, at different depths, to acquire bottle samples that were filtered to determine SSC by mass. The observed acoustic backscatter at the sampler location was simultaneously noted in the field. This allowed the determination of a best-fit equation relating the two variables. The relationship was assumed to follow the form:

$$\log_{10} \text{SSC} = A * \text{BS} - B \quad (4)$$

where BS is the measured backscatter intensity (dB), corrected for attenuation with range from the instrument, SSC is the sediment concentration (mg L^{-1}), and A and B are empirically derived coefficients.

One of the three study sites is near a long-term measurement station maintained by the U.S. Geological Survey (Station 11336930 Mokelumne River at Andrus Island near Terminous CA), and samples are collected there intermittently to quantify suspended sediment concentrations and percent fines, with sediment finer than $63 \mu\text{m}$ classified as fines. Of the 33 samples collected between 2012 and 2019, percent fines ranged from 75 to 100, with a mean of 93 and standard deviation of 7. Only eight values fell below 90, and low values are more likely during high flow events that were not surveyed as a part of this study for safety and logistical reasons.

The empirical coefficients appearing in Eq. (4) were assumed to be time independent. A separate analysis considering shallow vs. deeper samples revealed that sound attenuation due to sediment in the upper part of the water column had a negligible effect on the resulting best-fit equation: the result based on the shallow samples matched that for the entire collection.

For each transect, the appropriate equation was used to convert acoustic backscatter to SSC, and multiplied by the corresponding velocity vector, and integrated as in Eq. (1) to get net sediment flux. Corrections similar to those applied to the water fluxes (Eqs. (2) and (3)) were used to similarly correct computed sediment fluxes:

$$Q_s^+ = Q_{s_{\text{raw}}}^+ - \frac{\Delta Q_w}{2} * \frac{Q_s^+}{Q_w^+} \quad (5)$$

$$Q_s^- = Q_{s_{\text{raw}}}^- - \frac{\Delta Q_w}{2} * \frac{Q_s^-}{Q_w^-} \quad (6)$$

where subscript *s* denotes sediment fluxes, which are expressed as mass per unit time. Since the ratio of Q_s to Q_w is simply the mean sediment concentration, this approach involves multiplying the mean sediment concentration for the inflow or outflow portions of the transect by the correction to the water fluxes.

The ADCP must be submerged for operation and cannot measure within a small distance of its face. The earliest measurements were performed from a center console powerboat with a side-mounted ADCP, and instrument draft was ~ 60 cm. A customized kayak was used for most observations, with instrument draft of ~ 15 cm. Depending on vessel, the unmeasured zone, including the instrument blanking distance, thus spanned 30–90 cm at the top of the water column. Likewise, a region near the bed was left unmeasured. Bin size (the vertical resolution of the reported velocity and backscatter) was set at 25 cm. Water fluxes in the unmeasured regions were estimated using the instrument manufacturer's WinRiver II software (Teledyne 2019), which extrapolates a theoretical velocity profile up and down. At each location around the transect, these fluxes were multiplied by the mean of the top or bottom three computed values of SSC, extrapolating SSC up or down as necessary and multiplying by estimated local water flux and integrating to determine sediment fluxes over the entire water column.

A trapping efficiency was defined, based on corrected net trapped and incoming sediment fluxes:

$$\eta_s = \frac{Q_{s_{\text{net}}}}{Q_{s_{\text{in}}}} = \frac{Q_s^+ + Q_s^-}{Q_s^+} \quad (7)$$

With this definition, efficiency should range from minus infinity (no sediment inflow, non-zero sediment outflow) to +1 (100% incoming sediment trapped). A zero value indicates no net erosion from within the control volume. Note also that since trapping efficiency is a dimensionless flux difference, it is insensitive to both calibration coefficients appearing in Eq. (4)—it is dictated primarily by the difference in mean backscatter between inflow and outflow regions of a transect. For the test case shown in Fig. 3, the computed trapping efficiency is +10%.

Integrated Sediment Trapping

The approach described above yields only an instantaneous trapping efficiency. Of greater interest is the amount of sediment (mass or volume) actually trapped by SAV over longer time scales. This was evaluated by making use of separate measurements of velocity at fixed points within vegetated patches, and observations of the total flux of water and sediment in the channel, available at 15-min intervals over a period of approximately 3 years at the Mokelumne River site (Fig. 1; see U.S. Geological Survey Station 11336930

Mokelumne River at Andrus Island near Terminous, California, <https://waterdata.usgs.gov/>).

Separate measurements by Lacy et al. (2020) of velocity inside flow patches in the same region, made using fixed-mount ADV (acoustic Doppler velocimetry) instrumentation, reveal that flow speeds inside the surveyed patches of SAV are reduced by 90–99%, compared with flow in the adjacent channels. On this basis, a flow efficiency was defined:

$$\eta_w = \frac{\text{Flow speed inside patch}}{\text{Flow speed outside patch}} \sim 0.01\text{--}0.1 \quad (8)$$

Using this definition, the flux of water onto a patch is:

$$Q_{w\text{in}} = \frac{\eta_w Q_{wT}}{A_{\text{chan}}} A_{\text{in}} = \eta_w V_{\text{chan}} A_{\text{in}} \quad (9)$$

where A_{in} is the vertical area over which flow enters the vegetated region, and V_{chan} is the mean velocity of the approaching flow, with total discharge Q_{wT} . An upper bound on the inflow area was estimated as the width of the patch, in the direction normal to the incident flow, times the average water depth for the transect. This will be biased slightly high because the surveyed area, in planform, always exceeded that of the SAV patch, and depths inside the patch were often less than along the transect.

The rate of trapping of sediment within the patch can then be expressed in terms of the sediment trapping efficiency, the flow efficiency, the suspended sediment concentration C_s , and the influx of water:

$$Q_{s,\text{trapped}} = \eta_s \cdot \eta_w \cdot C_s \cdot V_{\text{chan}} \cdot A_{\text{in}} \quad (10)$$

This can be integrated in time numerically to determine cumulative sediment mass trapped:

$$M_{s,\text{trapped}} = \sum \eta_s \eta_w C_s(t) V_{\text{chan}}(t) A_{\text{in}} \Delta t \quad (11)$$

with 15-min time series of locally measured water flux and sediment concentration used as input. The two efficiencies and the inflow area were assumed constant when integrating. The higher flowrates and increased water levels that accompany storm events will likely increase the flow efficiency η_w and decrease the sediment trapping efficiency η_s , as SAV folds over in response to increased drag forces. At very high flowrates, the sign may even change on the sediment trapping efficiency, but field observations to prove this are not available.

Sediment Cores

Sediment cores were collected in *E. densa*-dominated SAV patches in April 2018 at the same three sites where flow and backscatter data were collected. Cores 60–80 cm in length were collected from a moored pontoon boat platform using a

gravity corer lined with 8.35 cm interior diameter cellulose tubing. Cores were sectioned in the field into 2-cm sections shortly after collection. Core sections were placed in labeled plastic bags and transported on ice.

Bulk density was determined by drying each core section at 60 °C for 72 h, weighing the section, and then dividing by the volume of the section. To determine percent organic matter, standard loss on ignition procedures were followed in which the dried bulk density samples were milled to 2 mm and heated to 550 °C for 4 h (Heiri et al. 2001). Characteristics of each 2-cm section can be found in Online Resources, Table S1.

Subsections of SAV cores were analyzed at a U.S. Geological Survey laboratory in Menlo Park, California, for ^{137}Cs , ^{210}Pb , and ^{226}Ra . Activities of total ^{210}Pb , ^{226}Ra , and ^{137}Cs were measured simultaneously by gamma spectrometry as described in Drexler et al. (2017). All radioisotope data for the cores can be found in Online Resources, Table S2. Radioisotope activities of subsections were measured using a high-resolution intrinsic germanium well detector gamma spectrometer. Samples were measured in the detector borehole, which provides near 4π counting geometry. Samples were all sealed in 7 mL polyethylene scintillation vials. The supported ^{210}Pb activity, which is defined by the ^{226}Ra activity, was determined on each core section from the 352- and 609-keV gamma emission lines of the short-lived daughters ^{214}Pb and ^{214}Bi daughters of ^{226}Ra , respectively. The activity of ^{137}Cs was determined from the 661.5-keV gamma emission line. Self-absorption of the ^{210}Pb 46-keV gamma emission line was determined and accounted for using an attenuation factor calculated from an empirical relationship between self-absorption and bulk density based on the method of Cutshall et al. (1983). Additional information regarding quality assurance/quality control can be found in Drexler et al. (2017).

SAV cores were dated using both ^{210}Pb and ^{137}Cs . For ^{210}Pb dating, the decay of the excess ^{210}Pb vs. cumulative dry mass was used (constant flux: constant sedimentation rate approach) to estimate a mean vertical accretion rate for each core (Appleby and Oldfield 1983; Drexler et al. 2017). The constant rate of supply model, which provides a unique accretion estimate for each section of a core, could not be used because the entire profile of excess ^{210}Pb was not recovered in the core profiles. Due to low activities of ^{137}Cs on the western coast of the USA and the possibility of mobility in the peat column (Drexler et al. 2018), we used ^{210}Pb exclusively for dating unless the only estimates available were from ^{137}Cs . ^{210}Pb values in the top 30 cm of cores were used to date core profiles because this depth range yielded the best results using the constant flux: constant sedimentation approach. The annual mass accumulation rate of all deposited material was estimated for each core by multiplying the vertical accretion rate determined using ^{210}Pb dating by the mean bulk density of the top 30 cm of the core. Uncertainties in ^{210}Pb dating were estimated following the method of Van Metre and

Fuller (2009). ^{137}Cs dating was only carried out if distinct ^{137}Cs peaks were found along the core profile. Vertical accretion rates were calculated by dividing the depth of the ^{137}Cs peak by the time period, x , between the date of core collection date and 1963 ($x = 55$ years for this study). Mass accumulation rates were determined by multiplying the mean bulk density of the top 30 m by the vertical accretion rate. Uncertainties in ^{137}Cs dating were estimated according to the approach of Drexler et al. (2017). The mean bulk density value and the estimated annual mass accumulation rate for each core are provided in Table 1.

Large-Scale Results and Long-Term Trends

Dividing the cumulative deposited sediment mass derived from acoustic velocity and backscatter data (Eq. 11) by the elapsed time and the planform area of the surveyed SAV patch yields the mass deposition per unit time per unit patch area. Lacking more definitive information, this was assumed representative of other patches. Multiplying by the total area of SAV in the Delta then yields an estimate of the net trapping of sediment by SAV per unit time. A related question is whether the trapping rate is changing over the long term.

The Mann-Kendall test (Mann 1945; Helsel and Hirsch 2002) was used to investigate long-term trends in sediment supply at two long-term flow stations, located at Freeport, on the Sacramento River, and Vernalis, on the San Joaquin River (Fig. 1). This is a non-parametric test for trend, applied in this case to time series of annual means of median daily values. Being non-parametric, it is influenced less than parametric tests by outliers in the time series.

The test was applied at both sites, to time series of discharge, suspended sediment concentration, and sediment flux, using the EGRET package for R software (Hirsch and De Cicco 2015). Daily observations were used to construct annual time series, and the Mann-Kendall test performed on the log of the variable of interest, at the annual scale. Tests with resulting p values less than 0.05 were considered significant, and the percentage change per year computed from the inferred trend.

The weighted regressions on time, discharge, and season (WRTDS) functionality within the EGRET package was used to investigate the dependence of suspended sediment concentration and percent fines in suspension on time and discharge. This approach involves the development of a regression model to fit observations of the constituent of interest and using the model to make predictions for unobserved moments or conditions. It can thereby reveal not only trends but the discharges or seasons during which they are most evident.

Results

The best-fit coefficients used in Eq. (4) to convert backscatter to SSC are shown in Table 2, with separate results for the Lindsey Slough and Mokelumne River sites. The relationship between backscatter and SSC at the Old River site was assumed the same as at the Mokelumne River site. The differences between the two best-fit equations are very small and a fit to the entire data set ($n = 29$, Fig. 4) is thus similar. R^2 ranges from 0.72 to 0.74 and residuals appear to be distributed about the best-fit line randomly and symmetrically. This is important because it means that when results are integrated spatially, random errors in computed SSC will tend to cancel one another. Also note that if one is interested in trapping efficiency, results are relatively insensitive to both coefficients, since efficiency is defined as net sediment flux divided by incident flux. For a simplified case including only one inflow and one outflow observation, with the same water flux at both sections, and high backscatter, the second coefficient in Eq. (4) vanishes upon subtraction to compute net flux, and the first vanishes upon division.

Applying Eq. (7) for trapping efficiency to data from each surveyed transect and screening to eliminate cases where water flux did not balance within 15% resulted in a total of 29 cases, 12 obtained during flood tide, and 17 during ebb tide. Trapping efficiency ranged from -8.4 to $+33\%$, with mean and median values of $+5.3$ and $+4.4\%$ respectively (Table 3). Only five of the 29 results for sediment trapping efficiency were negative, all but one of these occurring during flood tide. This one exception is unusual, however, in that pumps for

Table 1 Mean bulk density (\pm standard deviation) and estimated mass accumulation rates (\pm propagated dating error) for the top 30 cm of cores collected under submerged aquatic vegetation (SAVC) at Lindsey Slough (LS), Mokelumne (MOK), and Middle River (MR) in the Delta

Sediment core	Bulk density (g cm^{-3})	Mass accumulation rate ($\text{kg m}^{-2} \text{ year}^{-1}$)
LSSAVC1	0.407 ± 0.156	1.504 ± 0.691
LSSAVC2	0.420 ± 0.136	4.201 ± 2.017
MOKSAVC1	1.001 ± 0.226	6.007 ± 0.200
MOKSAVC3	0.939 ± 0.319	6.291 ± 0.187
MRSAVC1	0.271 ± 0.110	3.608 ± 1.519
MRSAVC2	0.299 ± 0.118	1.314 ± 0.597
Mean	0.556 ± 0.326	3.821 ± 2.132

Additional data for each 2-cm core section are provided in Online Resources, Tables S1 and S2

Table 2 Coefficients in Eq. 4 to compute SSC from acoustic backscatter

Site	A	B	n	R ²
Lindsey Slough	0.0404	-1.60	16	0.722
Mokelumne River, Old River	0.0393	-1.26	13	0.745

n, number of samples that went into derivation of each best-fit equation

pulling water supply often reverse the mean flow direction from what it would otherwise be at that site (Old River)—net flow is in the flood tide direction.

An attempt was made to investigate repeatability of the measurements, recognizing that the flow changes between measurements due to the tides. One patch of SAV in the Mokelumne River was circumnavigated five times over the course of 4 h, as the flow changed from ebb to flood. Computed trapping efficiencies were, in chronological order, 7.6, 1.3, 1.8, 8, and 5.1%, with the first two of these being during the ebb flow. Each result corresponds to different flow conditions, with inflow Q_w^+ ranging from 29 to 47 m³ s⁻¹ between the five observations. No correlation between the inflow and trapping efficiency was found for this period, so the range of values is concluded to be indicative of the magnitude of random errors inherent in the methodology. The results do suggest positive trapping efficiencies for both ebb and flood flows at the Mokelumne River site during the measurement campaign.

Table 3 Computed sediment trapping efficiency at three surveyed sites

Location	n	Sediment trapping efficiency (η_s , %)					
		Range		Mean		Median	
		Ebb	Flood	Ebb	Flood	Ebb	Flood
Lindsey Slough	4	NA	2.4–9.9	NA	7.1	NA	8.1
Mokelumne River	20	0.04–33	-4.8–8	7.4	3.6	5	5.7
Old River	5	-1.9	-8.4–7.8	-1.9	-1.0	-1.9	-1.8
All	29	0.04–33	-8.4–9.9	7.4	3.2	5	5.7

n, number of results

The gross flux of water through the measurement cylinder divided by the planform area of the cylinder was tested as a proxy for the mean velocity through the measurement domain, in order to investigate the influence of flow speed on trapping efficiency. Figure 5 depicts a typical measurement scenario, with the survey vessel circumnavigating a patch, by necessity including within the cylinder some areas that are unvegetated. Flow that takes place inside of the closed transect but outside of the vegetated patch biases the computed mean velocity high, and the trapping efficiency low, assuming that unvegetated areas are less efficient at slowing the flow and trapping sediment. These biases should vanish when the transect loop exactly follows the vegetated patch footprint. In the field, attempts were made to do this, but the patch was not always visible to the boat operator, who

Fig. 4 Empirical relationship between acoustic backscatter and SSC, based on 29 samples

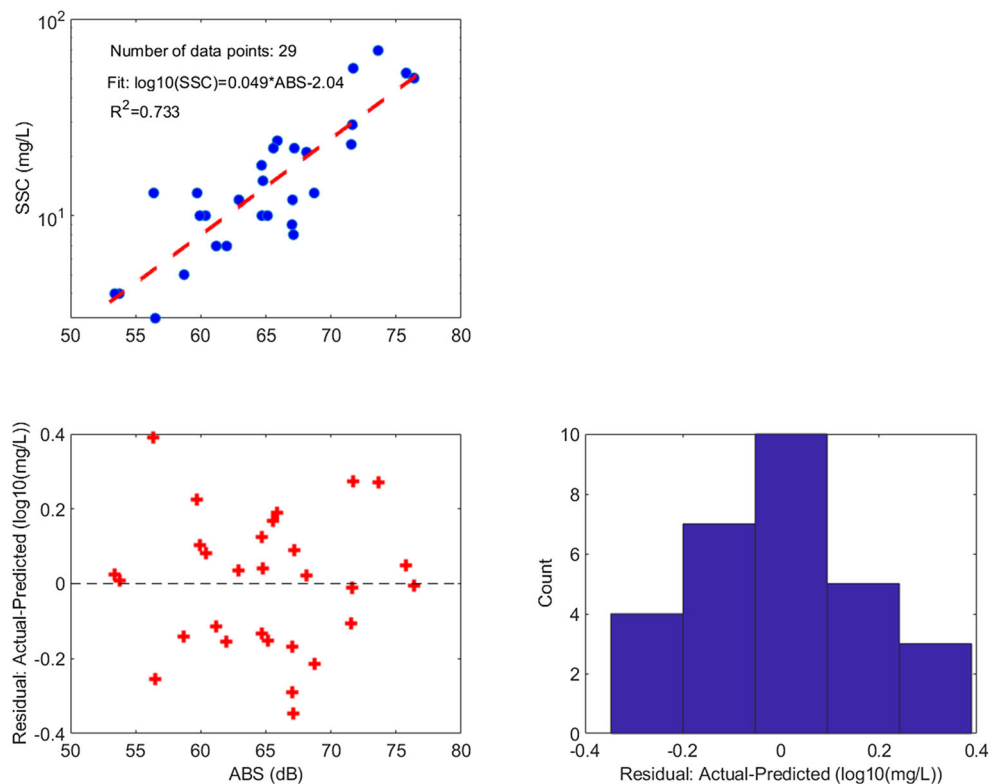
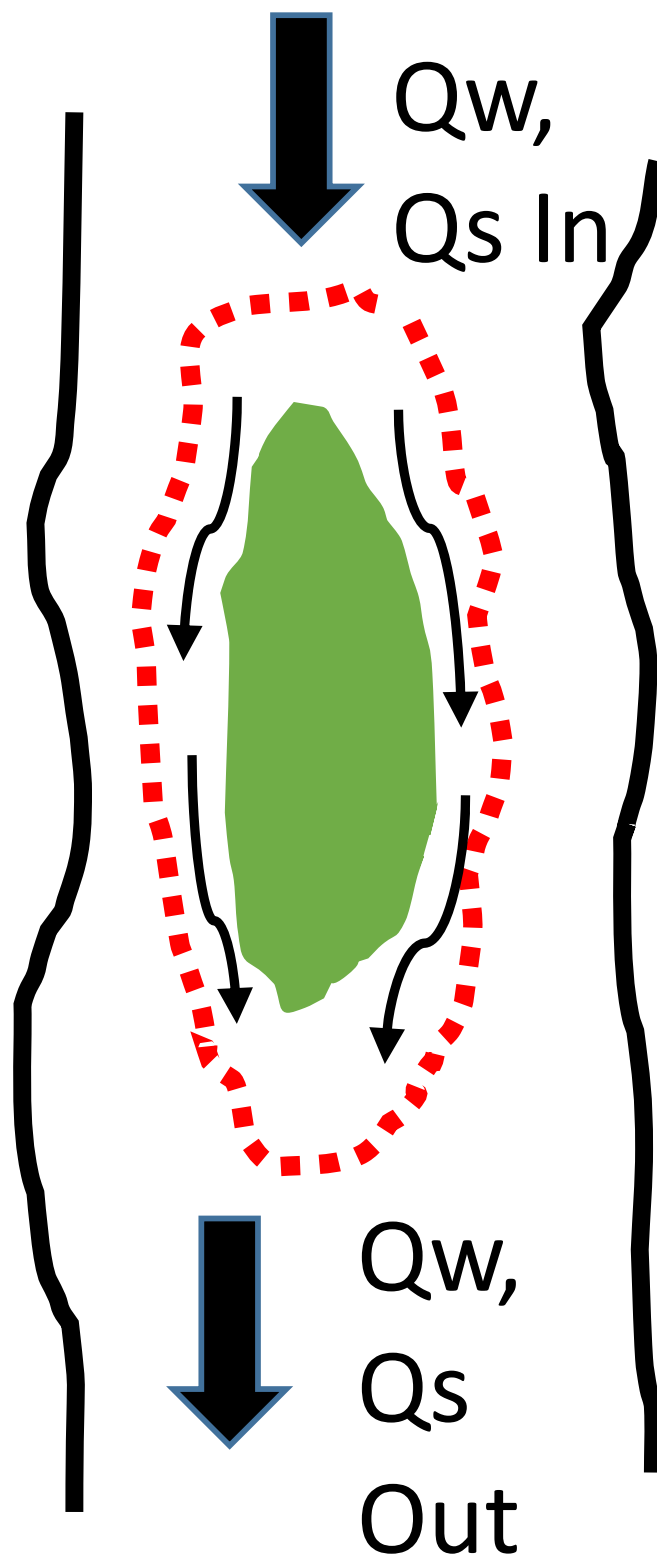


Fig. 5 Schematic plan view of transecting scenario, with red dotted line denoting boat track around patch of SAV (green). Solid black lines denote channel banks, and arrows are water and sediment flux vectors



often had to attempt to follow a depth contour using a fathometer. In practice, the operator had to choose a conservative path around but not into the SAV, because forays into vegetated areas resulted in data loss and rejection of results.

Gross flux of water divided by patch area was not correlated with sediment trapping efficiency (linear regression yields $R^2 = 0.0014$, $p = 0.85$). A separate, nearby measurement of cross-sectionally averaged velocity

was also investigated for correlation with trapping efficiency.

The Mokelumne River site is near a real-time flow measurement station (USGS station 11336930; see waterdata.usgs.gov). Figure 6 shows computed sediment trapping efficiency vs. simultaneous mean flow speed measured at this station. In all but one case at this site, trapping efficiency is positive, and trapping efficiency and flow speed appear to co-vary, but flow speed by itself is not a predictor of trapping efficiency ($R^2 = 0.13$, $p = 0.11$). There was a weak inverse correlation between sediment trapping efficiency and cross-sectionally averaged SSC observed at the measurement station ($R^2 = 0.18$, $p = 0.066$). Trapping efficiency was not correlated with sediment flux ($R^2 = 0.052$, $p = 0.33$). Like flow speed, SSC and sediment flux may have a second-order influence on sediment trapping efficiency, or the range of observed values may be too small to resolve its influence.

Equation (11) for computation of mass deposition inside a vegetated patch was applied at the Mokelumne River site, using a mean measured sediment trapping efficiency of 6.7% (Table 3), flow efficiency of 5% (Eq. 8), measured inflow area of 327 m², and planform area of the patch 57,500 m². Taking flow and SSC data for water year 2018 from USGS station 11336930, and integrating over the year via Eq. 11, yields 18 kt of sediment incident on the vegetated patch during the year. But only $0.067 * 0.05 = 0.3\%$ of this is trapped in the patch. The corresponding mass deposited in the patch within the year is 59 t, or 1.0 kg m⁻². The previous year saw a much higher flux of sediment past the site, with 6.9 kg m⁻² deposition computed. Repeating the calculation for the 3-year period (2016–2019) for which SSC measurements are available at the site yields a mean trapping rate of 3.7 kg m⁻² year⁻¹. Time series describing incident sediment flux at the other two sites are not available, which is why the field campaign emphasized the Mokelumne River site. The

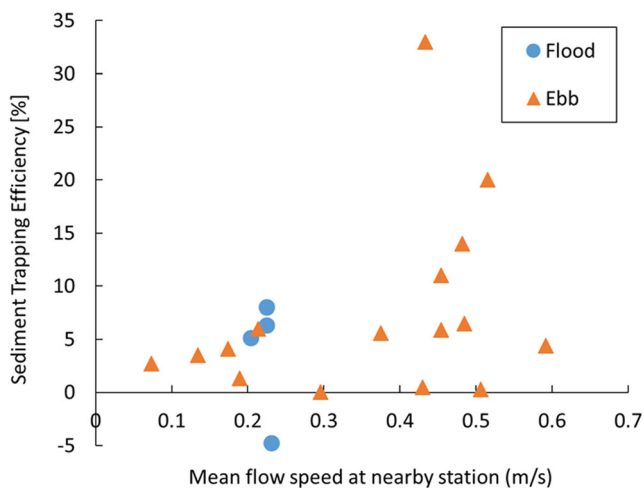


Fig. 6 Sediment trapping efficiency vs. cross-sectionally averaged flow speed at USGS Mokelumne River real-time measurement station 11336930

estimated trapping efficiency and mass deposition rates are in general agreement with those found by Van der Deijl et al. (2017) for their accretionary site.

These results compare favorably to mass accumulation rates derived from dated sediment cores, remembering that the latter are derived from 30 cm of core and represent many years of deposition (Table 1). The mass accumulation rates of cores ranged between 1.314 and 6.291 kg m⁻² year⁻¹. The mean value of 3.821 kg m⁻² year⁻¹ agrees closely with the above independently derived estimate of 3.7 kg m⁻² year⁻¹.

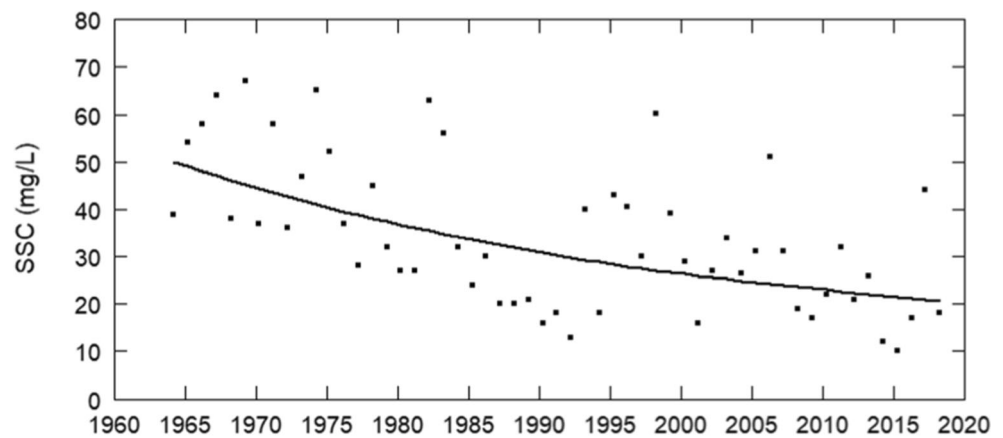
Data from two locations are available spanning a sufficiently long period (multiple decades) to conduct trend analysis on the supply of suspended sediment to the Delta. These are the USGS stations at Freeport, on the Sacramento River, between the city of Sacramento and the Delta, and at Vernalis, on the San Joaquin River, south of the Delta (Fig. 1). The two rivers are the largest contributors to the fresh water inflow to the Delta, and sediment flux data spanning more than 50 years are available at each site.

At Freeport, testing of long-term (1948–2019) annual discharge revealed a slight negative but statistically insignificant trend, which should be expected if the long-term average rainfall within the watershed has not changed. A flood bypass lies upstream of Freeport, receiving a large amount of winter storm flows, selectively reducing what would otherwise be the highest flows past the Freeport station. This bypass existed as a natural feature prior to the construction of levees and weirs around it, which were largely completed prior to the period of record considered here. The many reservoirs on upstream tributaries also help reduce peak flows past Freeport. Low flows are also heavily anthropogenically modified by water management decisions based on both water quantity and quality targets that dictate summer releases from upstream reservoirs.

A clear negative trend ($p = 0.00063$) was apparent in the SSC time series. Figure 7 shows the result based on the log of the annual mean value of the median daily SSC, with a 1.8% decrease in this parameter per year over the period 1963–2018. Similar trends were observed for analyses based on annual means of the minimum, maximum, and mean daily values, and the trend also exists when the concentration is normalized by annual discharge. With no meaningful trend in the annual discharge time series, and no significant change in the residuals of the discharge, a reduction in sediment availability is concluded as the reason for the downward trend in SSC over time, consistent with the findings of Wright and Schoellhamer (2005) and Schoellhamer et al. (2013), using a subset of the records employed here.

The WRTDS results for suspended sediment concentration, for the period 1973–2019 at Freeport, reveal that the long-term reduction in SSC occurred across all discharges and seasons. The change is most pronounced during winter high flows, which could be indicative of the effectiveness of

Fig. 7 Mann-Kendall test results for linear trend in the log of the mean annual value of median daily suspended sediment concentration (SSC) at USGS station 11447650, Sacramento River at Freeport, CA, water years 1963–2019. Trend is -1.8% year $^{-1}$, with $p = 0.00063$



flood control reservoirs at trapping sediment, reducing concentrations more significantly during periods of high concentration.

The sediment flux trends are similar to those for SSC. Mann-Kendall tests on the log of the annual mean of the daily median sediment flux values show a -2.2% per year change in sediment flux, with $p = 0.0252$. Similar results are found for the tests based on mean and maximum daily values. These results are consistent with those of Wright and Schoellhamer (2004) who considered the same datasets through the year 2001 and attributed much of the change to sedimentation within reservoirs built within the watershed. Hestir et al. (2016) noted similar trends in turbidity throughout the Delta and also concluded that the changes were a result of the combined effects of a reduction in sediment supply and an increase in sediment trapping as invasive SAV increased in abundance.

The coring data cited earlier also suggested some recent fining of the deposited material, prompting an investigation of the percentage of the sediment moving in suspension that is finer than sand (i.e., diameter < 0.063 mm). The patterns evident in the WRTDS results for percent fines in suspension at Freeport are subtle but also consistent with a reduction in the supply of fine sediment available for transport (Fig. 8).

Between 1990 and the onset of a major drought in 2012, there was a decrease in the percent fines in suspension. This trend appears to have reversed since then, perhaps in part because of upstream reservoir releases during large flow events that followed the drought. There is no significant trend in the mean annual value of the percent fines.

Figure 9 indicates that the change in percent fines in suspension does display a seasonal component, with large winter runoff events showing a trend toward increased percent fines, and summer months seeing a decrease. This too is consistent with the idea of a watershed that has a declining amount of fine sediment in riverbeds, downstream of reservoirs, and is receiving an increasing fraction of its fine sediment load from storm events, when reservoirs pass greater amounts of fine sediment downstream—while the total amount of sediment put into suspension decreases over time.

As with the Sacramento River watershed, the San Joaquin River watershed is very heavily modified, and influenced by water withdrawals. At the Vernalis station on the San Joaquin River (Fig. 1), the snowmelt signal is stronger than is observed at the Freeport site, with April–June discharge statistics similar to February–March statistics. The peak month for SSC is July.

Fig. 8 WRTDS result for percent fines in suspension at Freeport, 1973–2019. Color scale indicates percent fines. $n = 1103$ for percent fines and $n = 16,932$ for water discharge. Black lines show 5th and 95th percentile discharges, with unique values for each Julian day

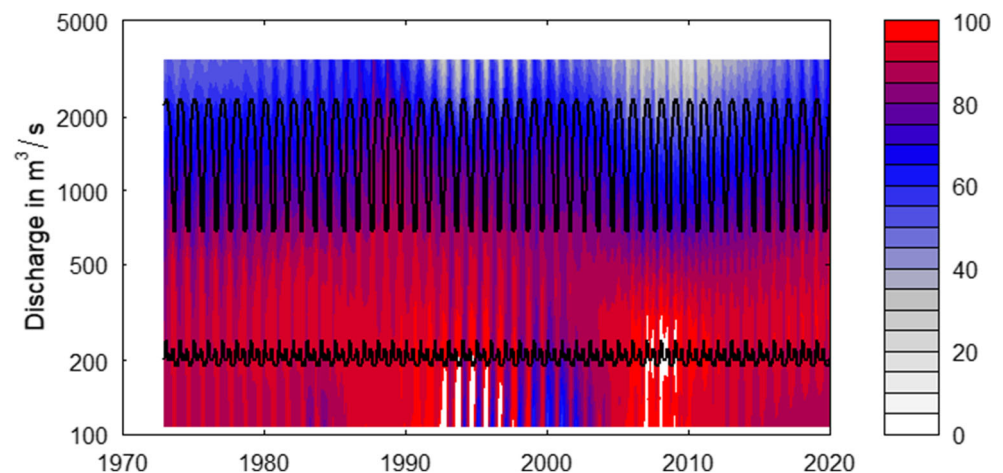
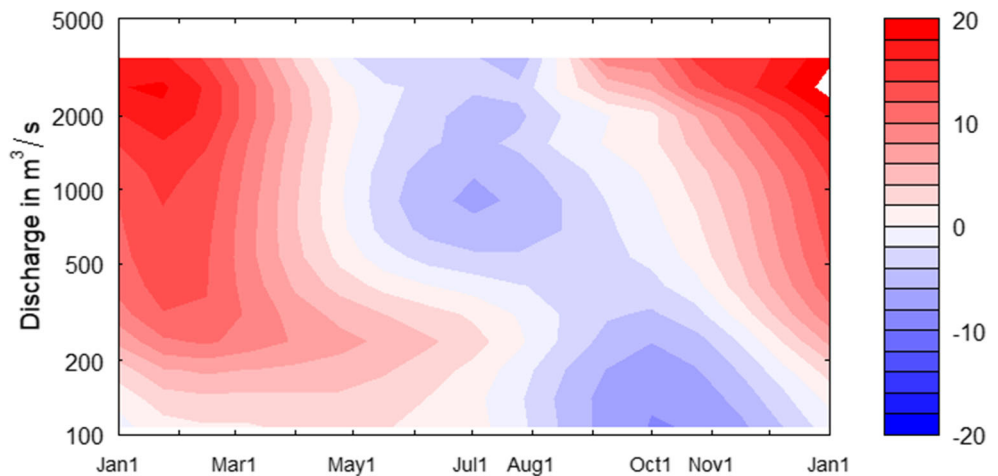


Fig. 9 Intra-annual variation in multi-decadal trend in percent fines in suspension at Freeport, 1973–2019. Color scale indicates change in percent fines in suspension over the period of record



Discharge data at Vernalis extend back to 1923. No significant trend was found in the annual discharge data. The SSC median daily values revealed a -1.1% annual change with $p = 8e-5$. The test on sediment flux was inconclusive. Note that the observed sediment flux at Freeport exceeds that at Vernalis by an order of magnitude.

Extrapolating the results shown here up to Delta-wide scale is difficult because of the time dependence in the many relevant parameters, the complicated nature of the flows of water and sediment, and their interaction with SAV as they pass over. But it is useful to attempt to reveal the big picture. With a sediment trapping efficiency of 5%, and a flow efficiency of 5%, an overall capture efficiency of 0.25% results. This means that 0.25% of the sediment carried by the incident flow over a patch becomes trapped inside.

To make use of this result, one also needs to know the sediment flux incident on a vegetated patch. For the one surveyed site at which this data was available the resulting annual deposition averaged $3.7 \text{ kg m}^{-2} \text{ year}^{-1}$ over a 3-year period. The Delta features invasive SAV over a third of its domain, with the SAV found preferentially in shallower sections. If the depths in these sections are 1/3 of the representative depth of the unvegetated areas, the vegetated patches will see approximately 10% of the total flow that passes by. Trapping 0.25% of 10% of the flow means that only 0.025% of the suspended sediment transport is being trapped. Deposition of $3.7 \text{ kg m}^{-2} \text{ year}^{-1}$ of suspended sediment on 21 km^2 (the 2015 estimate of the total area of invasive SAV) represents 82 kt year^{-1} of sediment that is unavailable to other areas where it may be needed.

Discussion

In this study, individual patches of invasive SAV were surveyed to provide the first direct estimates of instantaneous trapping efficiency regarding sediment in suspension.

Trapping efficiency was computed based on estimated fluxes of water and sediment through a closed transect surveyed by a roving vessel with a downward-looking acoustic Doppler current profiler, with acoustic backscatter used to estimate suspended sediment concentration. By using closed transects, error in net flux can be computed, and results for both water and sediment fluxes improved by forcing net water mass flux to zero, as required to conserve water mass.

Trapping efficiencies were positive—meaning that sediment is being actively trapped within the vegetated patch—in 24 of the 29 cases, which included three different tributaries and both ebb and flood flows. Trapping efficiency ranged from -8.4 to $+33\%$, with mean and median values of $+5.3$ and $+4.4\%$, respectively. Trapping efficiency was not found to be dependent on sediment concentration, or incident flow speed or sediment flux, but this may change once flow speeds exceed a threshold not encountered in this study.

It is important to note that several important assumptions were made when computing sediment trapping rates. Flow efficiency—the flow speed inside a patch divided by the speed outside—and sediment trapping efficiency were assumed constant, independent of time and flow conditions. Because of logistical and safety considerations, none of the field campaigns took place during major outflow events, although the coring and long-term SSC datasets include these events. With sufficiently high flow speeds, a vegetated patch may shift from being a sink to a source of sediment. For this reason, the sediment trapping efficiencies presented above should be considered an estimated upper bound, at least for riverine sites.

Flow speeds were found via a separate investigation to be reduced by 90–99%, compared to the incident flow speed (Lacy et al. 2020). Assuming an attenuation of 95% for the flow speed, and assuming that 10% of the flow cross-section is spanned by invasive SAV, it is estimated that 0.025% of the sediment in suspension is trapped by invasive SAV. This is a small fraction, but when converted to a dimensional quantity,

it represents a three-year mean of $3.7 \text{ kg m}^{-2} \text{ year}^{-1}$ of deposition, which agrees quite closely with the mean mass accumulation rate of $3.8 \text{ kg m}^{-2} \text{ year}^{-1}$ (Table 1) derived from sediment cores collected at the same study sites. It is important to consider that invasive SAV has been widespread in the Delta since the early 1990s (USDAARS-CDBW 2012). Currently, invasive aquatic vegetation (both SAV and floating aquatic vegetation) covers approximately 1/3 of the open water areas of the Delta (Khanna et al. 2018). Therefore, capture of suspended sediment by invasive SAV is likely significant on an area basis and therefore an important contributor to observed long-term reduction in suspended sediment concentration in the region (Schoellhamer et al. 2013).

The coring results presented here reflect the integrated effect of decades of sediment transport, but do not reveal trends within that period. Others have noted long-term changes in sediment supply to the Delta (e.g., Wright and Schoellhamer 2004), but since 2004 invasive SAV has increased in scope, likely influencing sediment supply downstream even further. Investigation of long-term trends in SSC and percent fines on the Sacramento River (the largest tributary to the Delta) revealed that sediment delivery to the Delta has continued to decline.

A clear long-term trend was apparent in the SSC record on the largest tributary to the area of interest, with a change in SSC of $-1.8\% \text{ year}^{-1}$ over the past six decades. This, despite no significant trend in long-term discharge. Some evidence of change in the intra-annual distribution of fine sediment in suspension was found, potentially attributable to (1) a long-term reduction in sediment supply, subsequent to nineteenth century inflows of sediment from hydraulic mining upstream and (2) the selective and time-dependent influence of flood control reservoirs on sediment in suspension.

Even though the results presented here suggest that only $\sim 0.025\%$ of the sediment arriving to the estuary is being trapped inside the invasive SAV, these two trends—reduced supply to and increased trapping within the estuary—mean that many parts of the estuary are receiving less and less sediment every year.

Any reduction of SSC has important implications for long-term marsh sustainability. In the Delta, microtidal freshwater marshes, which are typically comprised mainly of organic matter, require at least some inorganic sediment to maintain their position in the tidal frame (Drexler 2011). Marsh accretion modeling has shown that a reduction in suspended sediment will likely impede the ability of tidal freshwater marshes to maintain their elevation in the tidal frame, particularly under high rates of sea-level rise (Swanson et al. 2015). Further downstream in the brackish and saline marshes of the San Francisco Estuary, tidal range is greater and a larger proportion of inorganic sediment relative to organic matter is generally required for marsh-building. Sediment availability has been shown to be a major determinant of whether salt marshes

can remain sustainable or will ultimately drown under sea-level rise (Kirwan and Megonigal 2013; Schile et al. 2014). For these reasons, trapping of suspended sediment by invasive SAV represents another threat to the resilience of marshes to sea-level rise.

Acknowledgments We would like to thank Darin Einhell, Daniel Livsey, and David Schoellhamer (all of USGS California Water Science Center) for assistance with the field data collection and Shruti Khanna of the California Department of Fish and Wildlife for the remote sensing data.

Funding Information This work was funded by the U.S. Geological Survey (USGS) Priority Landscapes program. Mention of product names or manufacturers does not constitute an endorsement.

References

- Appleby, P.G., and F. Oldfield. 1983. The assessment of ^{210}Pb data from sites with varying sediment accumulation rates. *Hydrobiologia* 103 (1): 29–35.
- Asselman, N.E.M., and M. Van Wijngaarden. 2002. Development and application of a 1D floodplain sedimentation model for the River Rhine in the Netherlands. *Journal of Hydrology* 268 (1–4): 127–142.
- Champion, P.D., and C.C. Tanner. 2000. Seasonality of macrophytes and interaction with flow in a New Zealand lowland stream. *Hydrobiologia* 441 (1/3): 1–12.
- Chang, K., and G. Constantinescu. 2015. Numerical investigation of flow and turbulence structure through and around a circular array of rigid cylinder. *Journal of Fluid Mechanics* 776: 161–199. <https://doi.org/10.1017/jfm.2015.321>.
- Chanson, H., M. Takeuchi, and M. Trevethan. 2008. Using turbidity and acoustic backscatter intensity as surrogate measures of suspended sediment concentration in a small subtropical estuary. *J Environmental Mgmt* 88 (4): 1406–1416.
- Cutshall, N.H., I.L. Larsen, and C.R. Olsen. 1983. Direct analysis of ^{210}Pb in sediment samples: Self-absorption corrections. *Nuclear Instruments and Methods in Physics Research* 306: 309–312.
- Darke, A.K., and J.P. Megonigal. 2003. Control of sediment deposition rates in two mid-Atlantic Coast tidal freshwater wetlands. *Estuarine, Coastal and Shelf Science* 57 (1–2): 255–268.
- Downing-Kunz, M., Work, P.A., and Einhell, D., 2019. Sediment concentration and velocity data to assess trapping by submerged vegetation. U.S. Geological Survey data release, <https://doi.org/10.5066/P95R390Y>.
- Drexler, J.Z. 2011. Peat formation processes through the millennia in marshes of the Sacramento-San Joaquin Delta, CA, USA. *Estuaries and Coasts* 34 (5): 900–911.
- Drexler, J.Z., C.C. Fuller, J. Orlando, A. Salas, F.C. Wurster, and J.A. Duberstein. 2017. Estimation and uncertainty of recent carbon accumulation and vertical accretion in drained and undrained forested peatlands of the southeastern USA. *Journal of Geophysical Research – Biogeosciences* 122 (10): 2563–2579.
- Drexler, J. Z., Fuller, C.C., Archfield, S., 2018. The approaching obsolescence of ^{137}Cs dating of wetland soils in North America. *Quaternary Science Reviews*, <https://doi.org/10.1016/j.quascirev.2018.08.028>

- Durand, J., Fleenor, W., McElreath, R., Santos, M.J., Moyle, P., 2016. Physical controls on the distribution of the submersed aquatic weed *Egeria densa* in the Sacramento–San Joaquin Delta and implications for habitat restoration. *San Francisco Estuary and Watershed Science*, 14(1), article 4.
- Edwards, T.K., and Glysson, G.D., 1999. Field methods for measurement of fluvial sediment. U.S. Geological Survey Techniques of Water-Resources Investigations, book 3, chap. c2, 89 p. <http://water.usgs.gov/pubs/twri/twri3-c2/>.
- Federal Interagency Sedimentation Project, 2015. Operator's manual for the U.S. P-61-A1 point-integrating suspended sediment sampler. https://water.usgs.gov/fisp/docs/Instructions_US_P-61-A1_030115.pdf.
- Ganju, N.K., N.J. Nidzicko, and M.L. Kirwan. 2013. Inferring tidal wetland stability from channel sediment fluxes: Observations and a conceptual model. *Journal of Geophysical Research - Earth Surface* 118 (4): 2045–2058. <https://doi.org/10.1002/jgrf.20143>.
- Ganju, N.K., Z. Defne, T. Eelsey-Quirk, and J.M. Moriarty. 2019. Role of tidal wetland stability in lateral fluxes of particulate organic matter and carbon. *Journal of Geophysical Research – Biogeosciences* 124 (5): 1265–1277. <https://doi.org/10.1029/2018JG004920>.
- Getsinger, K.D., and C.R. Dillon. 1984. Quiescence, growth and senescence of *Egeria densa* in Lake Marion. *Aquatic Botany* 20 (3–4): 329–338.
- Gonzales, H.B., S. Ravi, J. Li, and J.B. Sankey. 2018. Ecohydrological implications of aeolian sediment trapping by sparse vegetation in drylands. *Ecohydrology* 11 (7): e1986. <https://doi.org/10.1002/eco.1986>.
- Gross, G. 1987. A numerical study of the air flow within and around a single tree. *Boundary-Layer Meteorology* 40 (4): 311–327. <https://doi.org/10.1007/BF00116099>.
- Heiri, O., A.F. Lotter, and G. Lemcke. 2001. Loss on ignition as a method for estimating organic and carbonate content in sediments; reproducibility and comparability of results. *Journal of Paleolimnology* 25 (1): 101–110.
- Helsel, D.R., Hirsch, R.M., 2002. Statistical methods in water resources. U.S. Geological Survey, Techniques of Water-Resources Investigations Book 4, Chapter A3.
- Hestir, E.L., D.H. Schoellhamer, T. Morgan-King, and S.L. Ustin. 2013. A step decrease in sediment concentration in a highly modified tidal river delta following the 1983 El Niño floods. *Marine Geology* 345: 304–313.
- Hestir, E.L., D.H. Schoellhamer, J. Greenberg, T. Morgan-King, and S.L. Ustin. 2016. The effect of submerged aquatic vegetation expansion on a declining turbidity trend in the Sacramento–San Joaquin River Delta. *Estuaries and Coasts* 39 (4): 1100–1112. <https://doi.org/10.1007/s12237-015-0055-z>.
- Hirsch, R.M., and De Cicco, L.A., 2015. User guide to exploration and graphics for river trends (EGRET) and data retrieval—R packages for hydrologic data (version 2.0, February 2015). U.S. Geological Survey Techniques and Methods book 4, chap. A10, 93 p., <https://doi.org/10.3133/tm4A10>.
- Huthoff, F., D.C.M. Augustijn, and S.J.M.H. Hulscher. 2007. Analytical solution of the depth-averaged flow velocity in case of submerged rigid cylindrical vegetation. *Water Resources Research* 43 (6): W06413. <https://doi.org/10.1029/2006WR005625>.
- Ingebritsen, S.E., M.E. Ikehara, D.L. Galloway, and D.R. Jones, 2000. Delta subsidence: The sinking heart of the state. Fact sheet FS-005-00, U.S. Geological Survey, 4 pp., <https://pubs.usgs.gov/fs/2000/fs00500/pdf/fs00500.pdf>
- Jones, J.I., A.L. Collins, P.S. Naden, and D.A. Sear. 2012. The relationship between fine sediment and macrophytes in rivers. *River Research and Applications* 28 (7): 1006–1018.
- Khanna, S., M.J. Santos, J.D. Boyer, K.D. Shapiro, J. Bellvert, and S.L. Ustin. 2018. Water primrose invasion changes successional pathways in an estuarine ecosystem. *Ecosphere*. <https://doi.org/10.1002/ecs2.2418>.
- Khanna, S., Acuna, S., Contreras, D., Griffiths, W.K., Lesmeister, S., Reyes, R.C., Schreier, B., Wu, B.J., 2019. Invasive aquatic vegetation impacts on Delta operations, monitoring, and ecosystem and human health. IEP Newsletter, Interagency Ecological Program, Sacramento, CA, 36(1), 8–19.
- Kim, H.S., I. Kimura, and M. Park. 2018. Numerical simulation of flow and suspended sediment deposition within and around a circular patch of vegetation on a rigid bed. *Water Resources Research* 54 (10): 7231–7251. <https://doi.org/10.1029/2017WR021087>.
- Kirwan, M.L., and J.P. Megonigal. 2013. Tidal wetland stability in the face of human impacts and sea-level rise. *Nature* 504 (7478): 53–60.
- Lacy, J.R., and S. Wyllie-Echeverria. 2011. The influence of current speed and vegetation density on flow structure in two macrotidal eelgrass canopies. *Limnology and Oceanography: Fluids and Environments* 1 (1): 38–55.
- Lacy, J.R., Ferreira, J.C.T., Dailey, E.T., Dartnell, P., Drexler, J.Z., Allen, R.M., Stevens, A., 2020. Sediment transport and aquatic vegetation data from three locations in the Sacramento–San Joaquin Delta, California, 2017 to 2018. U.S. Geological Survey data release, <https://doi.org/10.5066/P9112AIP>.
- Landers, M.N., Straub, T.D., Wood, M.S., Domanski, M.M., 2016. Sediment acoustic index method for computing continuous suspended-sediment concentrations. U.S. Geological Survey Techniques and Methods 3-C5, <https://doi.org/10.3133/tm3C5>
- Mann, H.B. 1945. Nonparametric test against trend. *Econometrica* 13 (3): 245–259.
- Nepf, H. 2012. Flow and transport in regions with aquatic vegetation. *Annual Review of Fluid Mechanics* 44 (1): 123–142. <https://doi.org/10.1146/annurev-fluid-120710-101048>.
- Ozturk, M. 2018. Sediment size effects in acoustic Doppler velocimeter-derived estimates of suspended sediment concentration. *Water* 2017 (9): 529. <https://doi.org/10.3390/w9070529>.
- Petticrew, E.L., and J. Kalf. 1992. Water flow and clay retention in submerged macrophyte beds. *Canadian Journal of Fisheries and Aquatic Sciences* 49 (12): 2483–2489.
- Rasmussen, P.P., Gray, J.R., Glysson, G.D., Ziegler, A.C., 2009. Guidelines and procedures for computing time-series suspended-sediment concentrations and loads from in-stream turbidity-sensor and streamflow data. U.S. Geological Survey Techniques and Methods book 3, chap. C4, 53 p.
- Rouse, H. 1937. Modern conceptions of the mechanics of fluid turbulence. *Trans Amer Soc Civ Eng* 102: 463–543.
- Sand-Jensen, K. 1998. Influence of submerged macrophytes on sediment composition and near-bed flow in lowland streams. *Freshwater Biology* 39 (4): 663–679.
- Schile, L.M., J.C. Callaway, J.T. Morris, D. Stralberg, V.T. Parker, and M. Kelly. 2014. Modeling tidal marsh distribution with sea-level rise: Evaluating the role of vegetation, sediment, and upland habitat in marsh resiliency. *PLoS One* 9 (2): e88760. <https://doi.org/10.1371/journal.pone.0088760>.
- Schoellhamer, D.H., S.A. Wright, and J.D. Drexler. 2013. Adjustment of the San Francisco estuary and watershed to decreasing sediment supply in the 20th century. *Marine Geology* 345: 63–71.
- Sheehan, M.R., and J.C. Ellison. 2015. Tidal marsh erosion and accretion trends following invasive species removal, Tamar Estuary, Tasmania. *Estuarine, Coastal and Shelf Science* 164: 46–55. <https://doi.org/10.1016/j.ecss.2015.06.013>.
- Simpson, M.R., Oltmann, R.N., 1993. Discharge-measurement system using an acoustic Doppler current profiler with applications to large rivers and estuaries. Water Supply Paper 2395, <https://doi.org/10.3133/wsp2395>
- Stoesser, T., S.J. Kim, and P. Diplas. 2010. Turbulent flow through idealized emergent vegetation. *Journal of Hydraulic Engineering* 136

- (12): 1003–1017. [https://doi.org/10.1061/\(ASCE\)HY.1943-7900.0000153](https://doi.org/10.1061/(ASCE)HY.1943-7900.0000153).
- Swanson, K.M., J.Z. Drexler, C.C. Fuller, and D.H. Schoellhamer. 2015. Modeling tidal freshwater marsh sustainability in the Sacramento–San Joaquin Delta under a broad suite of potential future scenarios. *San Francisco Estuary and Watershed Science* 13 (1) <https://escholarship.org/uc/item/9h8197nt>.
- Tanino, Y., and H.M. Nepf. 2008. Laboratory investigation of mean drag in a random array of rigid, emergent cylinders. *Journal of Hydraulic Engineering* 134 (1): 34–41. [https://doi.org/10.1061/\(ASCE\)0733-9429\(2008\)134:1\(34\)](https://doi.org/10.1061/(ASCE)0733-9429(2008)134:1(34)).
- Teledyne, M. 2019. *WinRiver II software users guide*, 313 pp. Poway, CA: Teledyne RD Instruments.
- Turner, R.E., E.M. Swenson, and C.S. Milan. 2001. Organic and inorganic contributions to vertical accretion in salt marsh sediments. In *Concepts and controversies in tidal marsh ecology*, ed. M. Weinstein and D.A. Kreeger, 583–595. Dordrecht: Kluwer Academic Publishing.
- United States Department of Agriculture Agricultural Research Service/California Division of Boating and Waterways (2012). *Egeria densa* control program. <https://search.usa.gov/search?utf8=%E2%9C%93&affiliate=agriculturalresearchservice&query=Egeria+densa+Control+Program>.
- Van der Deijl, E.C., M. van der Perk, and H. Middelkoop. 2017. Factors controlling sediment trapping in two freshwater tidal wetlands in the Biesbosch area, the Netherlands. *Journal of Soils and Sediments* 17 (11): 2620–2636. <https://doi.org/10.1007/s11368-017-1729-x>.
- Van Metre, P.C., and C.C. Fuller. 2009. Dual-core mass-balance approach for evaluating mercury and 210Pb atmospheric fallout and focusing to lakes. *Environmental Science and Technology* 43 (1): 26–32.
- Vergne, A., J. LeCoz, C. Berni, and G. Pierrefeu. 2020. Using a down-looking multifrequency acoustic backscatter system (ABS) for measuring suspended sediments in rivers. *Water Resources Research* 56: e2019WR024877. <https://doi.org/10.1029/2019WR024877>.
- Vogel, R.L., B. Kjerfve, and L.R. Gardner. 1996. Inorganic sediment budget for North Inlet Marsh, South Carolina, USA. *Mangroves and Salt Marshes* 1 (1): 23–35. <https://doi.org/10.1023/A:1025990027312>.
- Walder, J.S. 2015. Dimensionless erosion laws for cohesive sediment. *Journal of Hydraulic Engineering ASCE* 142 (2): 04015047. [https://doi.org/10.1061/\(ASCE\)HY.1943-7900.0001068](https://doi.org/10.1061/(ASCE)HY.1943-7900.0001068).
- Wilcock, R.J., P.D. Champion, J.W. Nagels, and G.F. Croker. 1999. The influence of aquatic macrophytes on the hydraulic and physico-chemical properties of a New Zealand lowland stream. *Hydrobiologia* 416: 203–214.
- Wright, S.A., and D.H. Schoellhamer. 2004. Trends in the sediment yield of the Sacramento River, California, 1957–2001. *San Francisco Estuary and Watershed Science* 2 (2).
- Wright, S.A., and D.H. Schoellhamer. 2005. Estimating sediment budgets at the interface between rivers and estuaries with application to the Sacramento–San Joaquin River Delta. *Water Resources Research* 41: W09428.
- Zong, L., and H. Nepf. 2011. Spatial distribution of deposition within a patch of vegetation. *Water Resources Research* 47 (3): W03516. <https://doi.org/10.1029/2010WR009516>.